International Journal of Fatigue 76 (2015) 53–59

Contents lists available at ScienceDirect

International Journal of Fatigue

journal homepage: www.elsevier.com/locate/ijfatigue

Effect of sudden load decrease on the fatigue crack growth in cold drawn prestressing steel

J. Toribio [a,*], B. González [a], J.C. Matos [b], F.J. Ayaso [a]

[a] Department of Materials Engineering, University of Salamanca, E.P.S., Campus Viriato, Avda. Requejo 33, 49022 Zamora, Spain
[b] Department of Computing Engineering, University of Salamanca, E.P.S., Campus Viriato, Avda. Requejo 33, 49022 Zamora, Spain

ARTICLE INFO

Article history:
Received 30 October 2013
Received in revised form 5 December 2014
Accepted 6 January 2015
Available online 21 January 2015

Keywords:
Overload retardation effect
Loading sequences
Fatigue crack growth
Cold drawn prestressing steel
Crack tip opening displacement

ABSTRACT

This paper analyzes the overload retardation effect (ORE) on the fatigue crack growth (FCG) of cold drawn prestressing steel when different loading sequences are used. The ORE is more intense for elevated load decrease or for low initial stress intensity factor (SIF) range ΔK_0. A transient stage can be observed in the Paris curve (da/dN–ΔK) when the $K_{max}\Delta K$ value suddenly decreases, associated with the ORE and with the evolution of the plastic zone and compressive residual stresses near the crack tip. In tests with K_{max} decrease, a small zone appears related to FCG initiation, with a fatigue fractography resembling the tearing topography surface (TTS) mode, and associated with a decrease of crack tip opening displacement (CTOD).

1. Introduction

Fatigue crack growth (FCG) usually is generated by load sequences of random nature, thereby producing very complicated load spectra and often overload and underload phenomena. Therefore, variable amplitude loading sequences, depending of the combination of load parameters, specimen geometry, material properties, microstructure and environment, can produce retardation or acceleration with regard to FCG [1]. The cyclic plastic behaviour of the material is found to strongly affect the crack behaviour after an overload or an underload, the type of hardening is also of key importance: isotropic hardening is found to lower the effective part of the fatigue cycle, while kinematic hardening is found to increase it [2].

The appearance of an overload during fatigue produces retardation phenomena in the FCG. Such a deceleration reaches its maximum value after certain crack extension, asymptotically diminishing later up to a stabilized level [3], those phenomena being closely related to the residual plastic zone size [4]. The retardation effect is higher if the ratio of the maximum peak stress to the maximum baseline stress is increased [4] and if the baseline stress intensity factor (SIF) range ΔK is modified, either by increasing it (approaching the fracture toughness) or diminishing it (approaching the FCG threshold) [5].

Overload retardation effect (ORE) increases with the number of overload cycles [4,5] until it reaches a maximum value, existing a characteristic distance between overloads which ensures the greatest retardation effect [6]. In high-low block loading sequences the maximum ORE is instantaneous [5]. A single compressive peak load just after the tensile overload relaxed the overload effect [3] and can result in an acceleration in the rate of FCG [7].

The main reason for the retardation in overload crack advance, as well as the crack tip closure, are the crack branches and the contact between surfaces, of rough fracture, after overload [8]. The ORE is higher due to plasticity effects (for elevated ΔK) or because of asperity wedging (for low ΔK) [5]. A block of compressive overload cycles may cause ORE on the growth rate of the initial crack, due to the oxide-induced closure which generates debris [9]. On the other hand, other authors maintain that every deviation of large crack growth behaviour can be linked to the presence of residual stresses on the material [10].

This paper considers the two main driving forces for FCG: (i) the SIF range ΔK and (ii) the maximum SIF K_{max} [11], and analyzes the ORE caused by the sudden decrease of any of them on the FCG in cold drawn pearlitic steels. To this end, the following factors were considered: the ORE during FCG, the plastic zone size in the close vicinity of the crack tip, the appearance of the micro-tearing pattern in the fatigue fracture surface and the crack tip opening displacement (CTOD).

* Corresponding author. Tel.: +34 (980) 54 50 00; fax: +34 (980) 54 50 02.
E-mail address: toribio@usal.es (J. Toribio).

http://dx.doi.org/10.1016/j.ijfatigue.2015.01.007
0142-1123/

2. Experimental procedure

The material used in the study was high strength prestressing steel with eutectoid composition (0.789 wt.% C, 0.681 wt.% Mn, 0.210 wt.% Si, 0.218 wt.% Cr, 0.061 wt.% V, balanced with Fe) and pearlitic microstructure. Commercial prestressing steel wires are obtained from a hot rolled bar which is subjected to a cold drawing process in seven steps, thereby producing a high cumulative plastic strain ($\varepsilon^P = 1.6$) and activating a strain hardening mechanism to improve the conventional mechanical properties of the material. The resulting mechanical properties are as follows: yield strength $\sigma_Y = 1480$ MPa, tensile stress $\sigma_R = 1820$ MPa and Young modulus $E = 209$ GPa.

Fatigue tests were performed on wires of 300 mm of length and 5.1 mm of diameter, subjected to two cyclic loading sequences, each of one consisting of maintaining constant the two key mechanical parameters defining the fatigue cycle, namely (i) the stress range $\Delta\sigma$ and (ii) the maximum stress σ_{max} (and obviously σ_{min}), and a sudden decrease of either $\Delta\sigma$ or σ_{max} in the transition from the first to the second stage of loading. An axial cyclic tensile load was externally applied under a frequency of 10 Hz and using a sinusoidal wave in such a manner that the maximum stress was always maintain well below the material yield strength σ_Y. An extensometer of 25 mm gage length was placed on the specimen in symmetrical position in relation to the crack mouth, in order to monitor the crack length by means of the compliance ($C = u/F$, ratio of the relative displacement measure by the extensometer and the externally-applied remote tensile load). The designed test types appear sketched in Fig. 1: (i) in type A tests there is a decrease of maximum stress σ_{max}; (ii) in type B tests there is a decrease of stress range $\Delta\sigma$; (iii) in type C tests there is a decrease of both driving forces (σ_{max} and $\Delta\sigma$). In all types of tests (A, B and C) the subindex indicates the percentage of decrease in relation to the previous value.

The fracture surface corresponding to the sudden load changes was observed by optical microscopy and by scanning electron microscopy (SEM). Materialographic techniques (mounting, grinding, polishing and 5% Nital etching) were used to observe by SEM the microstructure of the prestressing steel. In addition, a fracto-materialographic procedure was used to evaluate the fatigue crack paths by interrupting the test before final fracture, cutting the specimen across a plane perpendicular to the crack front and applying metallographic techniques to observe the evolution of the crack immersed in the microstructure.

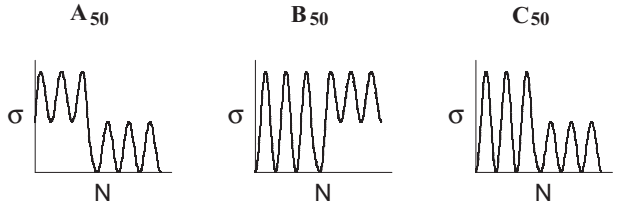

Fig. 1. Tests with 50% sudden load decrease.

3. Experimental results

3.1. Microstructural analysis

The microstructure of prestressing steel is constituted by pearlite colonies, each of one consisting of alternate lamellae of ferrite and cementite with common orientation inside the colony (such an orientation being different from that of the lamellae contained in any neighbourhood colony). Cold drawing produces effects in the two basic microstructural levels of the steels, namely, the pearlitic colony and the ferrite/cementite lamellae.

With regard to the first microstructural level (the pearlitic colony), there is a progressive orientation [12] with cold drawing (in direction quasi-parallel to the wire axis or drawing direction), together with a slenderization in the same direction [13]. While in the first stages of drawing the orientation effect is predominant, in the last drawing steps a marked slenderization and enlargement of the colonies takes place [12,13].

In the matter of the second microstructural level (the set of pearlitic lamellae), again a progressive orientation [14] appears with cold drawing (in direction quasi-parallel to the wire axis or drawing direction), in addition to the increase of packing closeness in the form of reduction of the interlamellar spacing of pearlite [15]. Whereas in the earlier steps of the process the orientation effect is relevant, in the further stages of drawing a marked decrease of spacing appears (accompanied by curling of the lamellae), cf. [14,15].

Fig. 2 shows the microstructure of prestressing steel wire in both transversal and longitudinal sections, where the afore-said effects associated with the final step of drawing (heavily drawn prestressing steel wire) can be observed, namely orientation of colonies and lamellae, reduced interlamellar spacing and enlargement of the colonies in the drawing direction.

3.2. Retardation in fatigue crack growth (FCG)

The FCG curve in the Paris regime, cyclic crack growth rate (CCGR) *vs.* the SIF range da/dN–ΔK, for the cold drawn pearlitic steel analyzed in this paper is shown in Fig. 3. The plot is the same for different values of the R ratio [16]; so CCGR depends mainly on the SIF range, while the maximum SIF during fatigue, K_{max}, is almost irrelevant. The Paris fitting gives coefficients C and m of

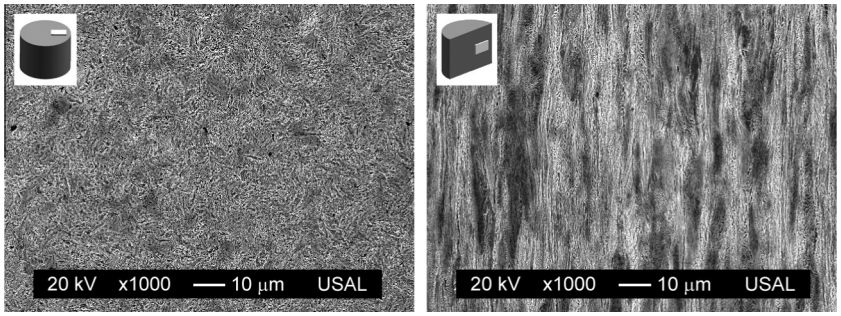

Fig. 2. Microstructure of prestressing steel wire: in the transversal section (left) and the longitudinal section (right). The horizontal side of the photograph is associated with the radial direction in the wire, whereas the vertical side of the photograph corresponds to the circumferential direction in the transversal section and to the axial direction in the longitudinal section.

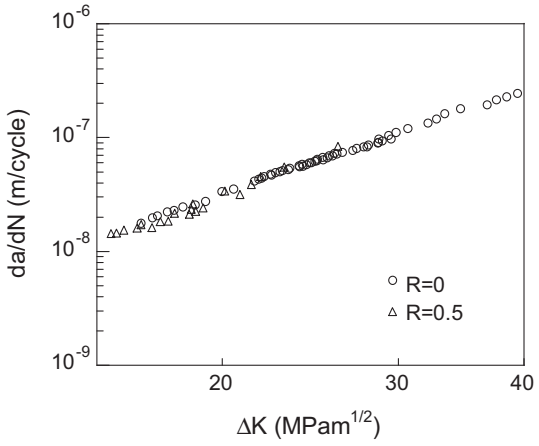

Fig. 3. da/dN–ΔK curve in the Paris regime.

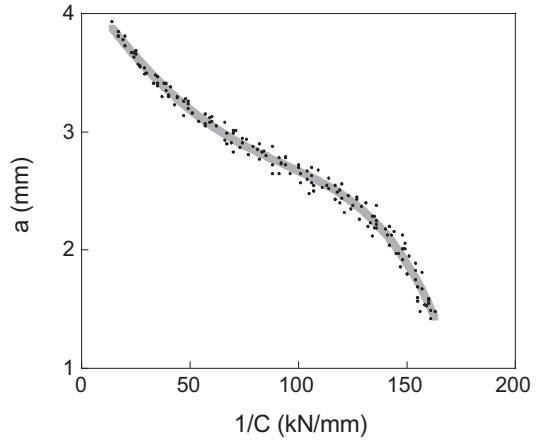

Fig. 4. Evolution of the relationship between the crack length and the inverse of the compliance $1/C$ during crack growth.

$4.1 \cdot 10^{-12}$ and 3.3 (da/dN given in m/cycle and ΔK in MPa $m^{1/2}$). According to the published scientific literature, some materials exhibit a strong R ratio dependency while others show a weak R ratio influence [17]. High strength steels display the latter behaviour, i.e. the da/dN *vs.* ΔK relationship shows no R ratio dependence in the Paris region II but appears to be R ratio dependent in the near-threshold region I [18].

During the fatigue tests on prestressing steel wires the crack front was characterized as a part of an ellipse with its center located at the wire periphery and semiaxes a (crack depth) and b (second parameter defining the crack shape). Fig. 4 allows one to obtain the crack length a at each instant as a function of the inverse of the compliance $1/C$.

The second cyclic loading sequence begins at the same crack length (measured through the compliance) in all tests, in order to avoid any size effect (or crack length effect) on tests results. In addition, the second loading block was developed always using the same $\Delta\sigma$ value in each group of experiments (two different $\Delta\sigma$ values were chosen for the second cyclic loading sequence). Thus, the CCGR would have been the same if the ORE did not exist.

Figs. 5 and 6 show the relationship between crack length and number of cycles (a–N) during the second loading sequence for the different types of test, with respective loading decrease of 50% and 30% and initial SIF range (at the beginning of that *second loading sequence*) ΔK_0 = 15 MPa $m^{1/2}$. Figs. 7 and 8 show the same plot for ΔK_0 = 27 MPa $m^{1/2}$ and respective decrease of 50% and 30%.

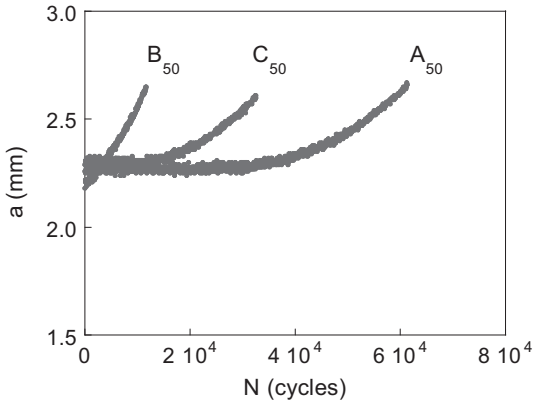

Fig. 5. Crack depth *vs.* number of cycles (a–N) for the second loading sequence, with 50% load decrease and initial SIF range ΔK_0 = 15 MPa $m^{1/2}$.

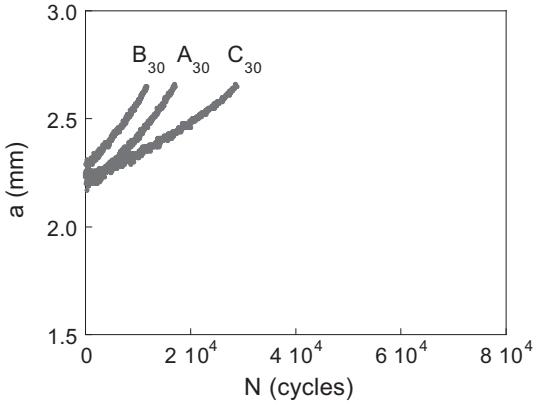

Fig. 6. Crack depth *vs.* number of cycles (a–N) for the second loading sequence, with 30% load decrease and initial SIF range ΔK_0 = 15 MPa $m^{1/2}$.

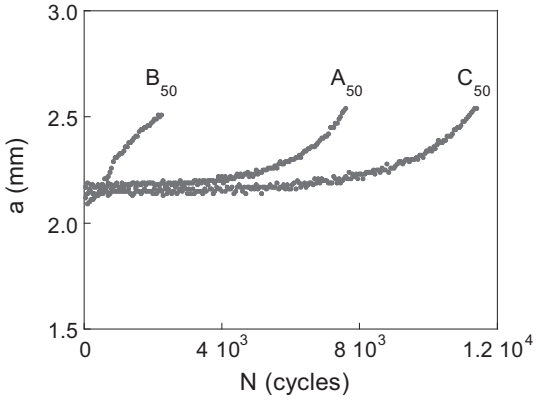

Fig. 7. Crack depth *vs.* number of cycles (a–N) for the second loading sequence, with 50% load decrease and initial SIF range ΔK_0 = 27 MPa $m^{1/2}$.

Considering all the experiments, it is seen that the B-type tests exhibit the minimum ORE in FCG, in spite of the sudden decrease of $\Delta\sigma$ in such a type of test. On the other hand, A- and C-type tests show a clear ORE in FCG, slight in the case of 30% load drop and more intense when the decrease of load between sequences is higher (50%). In the latter case the number of cycles required for crack initiation is relatively high and the effective SIF range for crack initiation (accounting for the effect of compressive residual

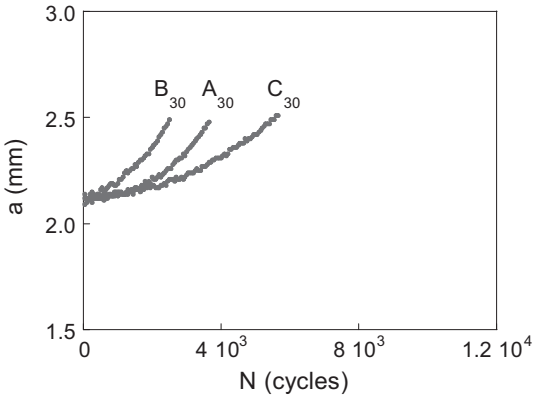

Fig. 8. Crack depth *vs.* number of cycles (a–N) for the second loading sequence, with 30% load decrease and initial SIF range ΔK_0 = 27 MPa m$^{1/2}$.

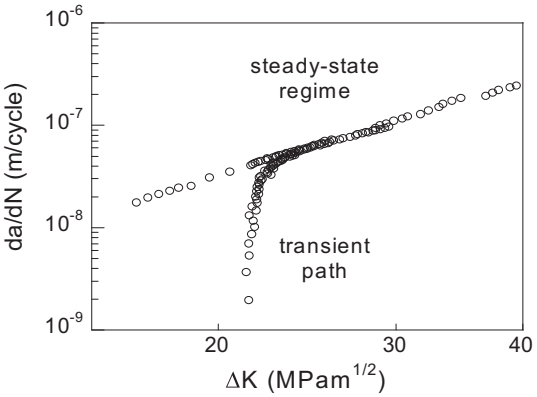

Fig. 9. da/dN–ΔK curve: steady-state regime + transient path.

stresses in the close vicinity of the crack tip) is closer to the threshold for FCG ΔK_{th}. In addition, according to previous research, it should be considered that threshold levels in FCG under variable amplitude loading can be different than the threshold values observed in constant amplitude tests [1]. Again in the matter of A- and C-type tests, the ORE in FCG is more intense when it takes place for lower values of ΔK_0 (15 MPa m$^{1/2}$), than when it happens for higher levels of ΔK_0 (27 MPa m$^{1/2}$).

Generally speaking, the ORE in FCG is more intense in C tests than in A experiments, with the exception of the test performed with low ΔK_0 (15 MPa m$^{1/2}$) and load decrease of 50% in which the opposite trend appears. Such a behaviour is an indication of the existence of several mechanisms operating in the vicinity of the crack tip and contributing to the ORE in FCG: development of local plasticity near the crack tip, constrain evolution in that area, changes in CTOD, etc.

4. Discussion

The discussion of the experimental results contained in this paper will be divided in three sections: (i) mechanical aspects of FCG, with special emphasis on the evolution of the plastic zone size; (ii) physical features of FCG, namely fractographic analysis of the fatigue surfaces, dealing with the microscopic aspect of the crack phases (roughness, microtearing, facets...); (iii) geometrical appearance of the near-tip profile, i.e. crack tip opening displacement (CTOD).

4.1. Evolution of the plastic zone size

The plastic zone and the compressive residual stresses near the crack tip can be considered as factors causing the transient state in the Paris law (Fig. 9), assuming that the mechanisms is similar to that governing ORE in FCG [19,20], in which the size of the plastic zone and the level of the compressive residual stresses are relevant magnitudes influencing the crack advance during each cycle.

The retardation is considered to be produced when the plastic zone created near the crack tip by the last cycles of the initial stress sequence with a given $\Delta\sigma$ (*primary plastic zone*) surrounds the smaller plastic zone caused by the (lighter) initial cycles of the following loading stage (*secondary plastic zone*), thereby retarding fatigue crack growth. The ORE is seen to depend on the number of overload cycles causing it [6], although the last stress cycle is the relevant one regarding the afore-said phenomenon. On the basis of these assumptions and in agreement with Ref. [21], the expression experimentally obtained for the plastic zone size of cold drawn pearlitic steel is the following,

$$r_p = 0.14 \frac{K_{max}\Delta K}{\left(\frac{\sigma_Y+\sigma_R}{2}\right)^2} \quad (1)$$

where the size of the plastic zone is linearly dependent on the product $K_{max}\Delta K$, i.e. both variables act as driving forces for FCG [11]. In addition, and considering than material exhibits strain hardening, mechanical properties (namely the yield strength σ_Y and the ultimate tensile stress σ_R of the cold drawn pearlitic steel used in this paper) are also parameters influencing the size of the plastic zone (r_p). The fitting coefficient of expression (1) was obtained as 0.14, in perfect agreement with the estimation of other models [22,23].

Fig. 10 shows the *primary plastic zone* (associated with the last cycle of the first loading sequence) and the *secondary plastic zone* (associated with the first cycle of the second loading sequence), calculated by using Eq. (1). On the basis of the analysis of the plastic zone size, one could establish certain *a priori* estimation of the

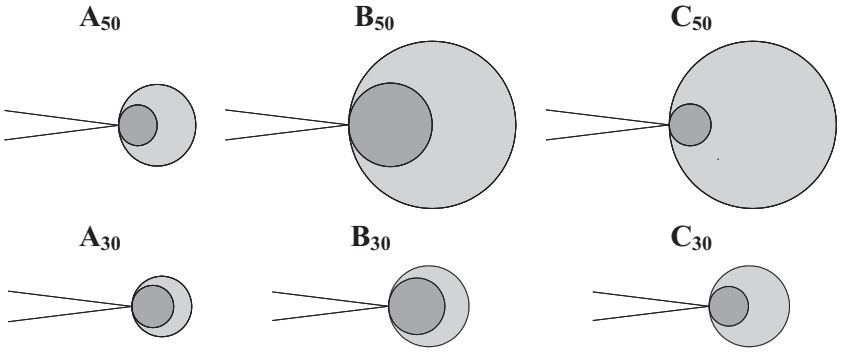

Fig. 10. Plastic zone size: *primary plastic zone* (light grey) and *secondary plastic zone* (dark grey).

possible ORE: it is seen (cf. Fig. 10) that the more intense ORE could be associated with the case in which the difference is higher between both plastic zone sizes, namely C-type tests with a sudden decrease of load of 50% (C_{50}). Following the *a priori* estimation, in the second place one could signal three types of test (A_{50}, C_{30} and B_{50}), and finally A_{30} and B_{30} in which the ratio between both plastic zone sizes (the *primary* and the *secondary*) is minimum, so that the ORE effect caused by compressive residual stresses in the vicinity of crack tip is less intense.

4.2. Fractographic analysis of the fatigue surfaces

Fig. 11 shows the fatigue fracture surfaces in the steels, for the A-, B- and C-type tests and 50% decrease of load. A well-defined semi-elliptical crack front can be observed on the fatigue surfaces in some experiments (A- and C-type tests), defining the transition between the two sequences of loading (and thus associated with the sudden load decrease). B-type tests represent an exception, because in this case the transition between the two fractographic areas linked with the two sequences of loading can hardly be observed in the form of a well-defined semielliptical crack front. The afore-said visible crack front can be caused by the sudden load decrease and its associated physical effect at the finest microscopic level.

The fatigue fracture surface in the analysed pearlitic steel resembles ductile micro-tearing events, probably related to plastic crack advance under cyclic loading. Micro-tearings in cold drawn pearlitic steel present a smaller size and more curved geometry than those in the hot rolled wire where it comes from [16], due to the microstructural changes (orientation of the pearlitic lamellae, curling of the lamellae in the transverse section and decrease of its interlamellar spacing, cf. Fig. 2) and to the plastic strain undergone by the steel during the drawing process.

Fig. 12 shows the fatigue fracture surfaces obtained by SEM for different regimes of cracking, exhibiting ductile micro-tearing patterns for several levels of fatigue intensity. This observations, together with the fact that in B-type tests (where K_{max} is constant) there are no fractographic changes at the microscopic level, support the assumption that the micro-tearing appearance is mainly determined by the maximum SIF during fatigue K_{max}, and very scarcely by the SIF range ΔK.

For A- and C-type tests the appearance of the fatigue fracture surface depends on the specific loading sequence. The area associated with the initiation of cracking just after the sudden decrease of load exhibits a particular fractography (Fig. 13) resembling micro-tearing, micro-damage or ductile events and oriented in the main direction of crack advance. Such a fractographic appearance represents a non-conventional micromechanical fracture mode defined as *tearing topography surface* (TTS), a term coined by Thompson and Chesnutt [24]. A magnification of this fractographic mode is shown in Fig. 14, in which the ductile

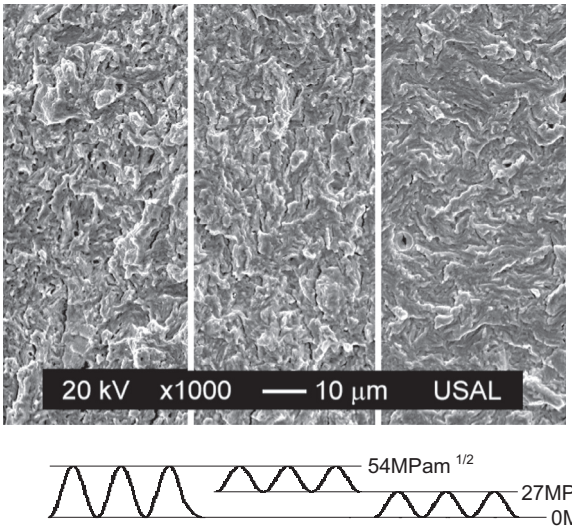

Fig. 12. Fractography: $K_{max} = \Delta K \sim 54$ MPa m$^{1/2}$ (left); $K_{max} \sim 54$ MPa m$^{1/2}$ and $\Delta K \sim 27$ MPa m$^{1/2}$ (center); $K_{max} = \Delta K \sim 27$ MPa m$^{1/2}$ (right). In all cases the fatigue crack advances from left to right.

micro-tearing (or micro-damage) events can be detected at a very fine scale of micrometers, and they are probably an evidence of plasticity-induced FCG, i.e. plastic crack advance under cyclic loading.

4.3. Crack tip opening displacement (CTOD)

A possible explanation of this region with initiation fractography is the sudden decrease of the CTOD at the beginning of the second step in several tests, causing a new crack from another one with such a CTOD that it can be considered a micro-notch. This phenomenon appears intensely in test A_{50}, where it was observed that the crack opening variation is very strong when the load level suddenly changes (Fig. 15).

The maximum CTOD δ_{max}, for a plane strain situation, may be estimated using the following expression,

$$\delta_{max} \approx \frac{K_{max}^2}{2\sigma_Y E} \tag{2}$$

where E is the Young modulus and σ_Y the yield strength of the material.

The cyclic CTOD $\Delta\delta t$ can also be estimated in similar way as follows,

$$\Delta\delta_t \approx \frac{\Delta K^2}{4\sigma_Y E} \tag{3}$$

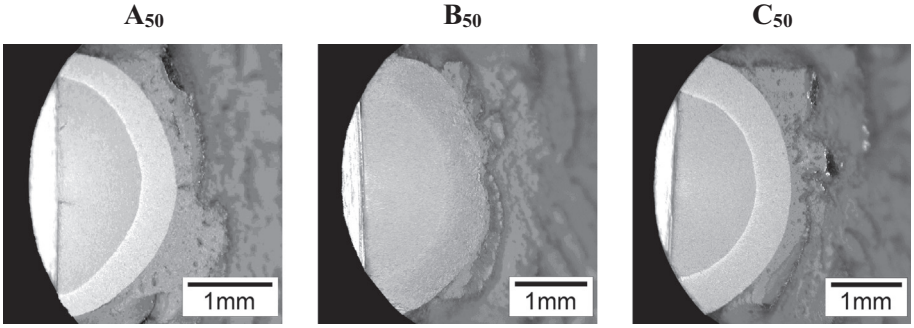

Fig. 11. Fatigue fracture surfaces for the A-, B- and C-type tests and 50% decrease of load (optical microscopy). The fatigue crack advances from left to right.

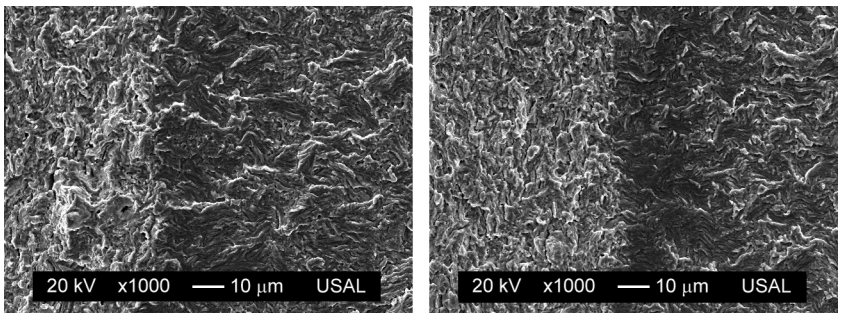

Fig. 13. Fractography: A_{50}-type test (left) and C_{50}-type test (right). The fatigue crack advances from left to right.

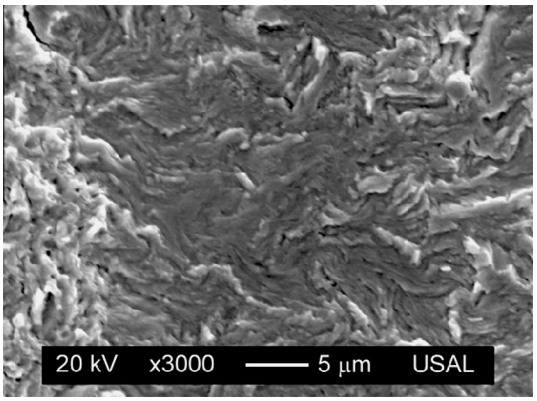

Fig. 14. Fractography of *tearing topography surface*, TTS, in A_{50}-type test. The fatigue crack advances from left to right.

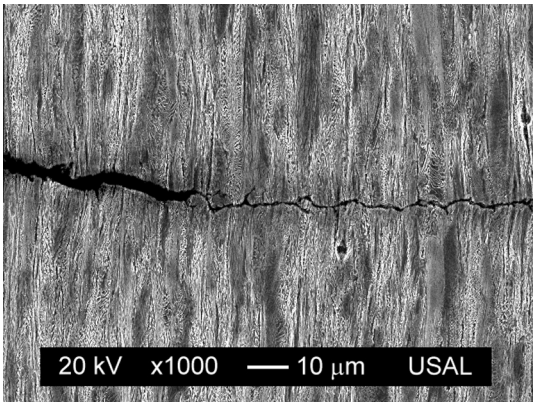

Fig. 15. Longitudinal cut (fracto-materialography) in A_{50}-type test, showing the fatigue crack paths. The crack advances from left to right.

On the basis of the above expressions, the CTOD change can be calculated from one sequence to the following one in all types of test. Fig. 16 shows a sketch of the approximate shape of the crack tip area in the two loading sequences. It can be observed that in A- and C-type tests the CTOD decreases when the sudden load change occurs, this phenomenon being stronger in test A_{50}, in which this effect was experimentally observed (see Fig. 15). On the other hand, in B-type tests there is a greater CTOD after the load change, as the fatigue surface shows in Fig. 11. The consequences of this fact is an ORE that is less pronounced than the expected one for this kind of test taking into account the plastic zone sizes.

4.4. The role of plasticity-induced crack closure (PICC)

Following Suresh [25], it is evident that PICC alone cannot explain the influence of various mechanical, microstructural and environmental factors on fatigue crack growth, especially in the near-threshold regime. Furthermore, recent research by Toribio and Kharin [26,27], consisting of high-resolution elastoplastic simulations of plane-strain tensile crack under cyclic loading, allows a visualization of the Laird–Smith scheme of crack growth by plastic blunting and re-sharpening. On the basis of these results, no signs of crack closure were detected. However, calculated plastic crack growth reproduced the key trends of FCG, such as the rate increase with ΔK and the arrest by an overload. This raises reasonable doubts concerning the ubiquitous presence and significance of PICC in the plane-strain fatigue cracking, as well as questions the deductions about PICC derived from the FCG data.

5. Conclusions

The following conclusions may be drawn regarding the influence of sudden load changes on the fatigue crack propagation in cold drawn prestressing steel:

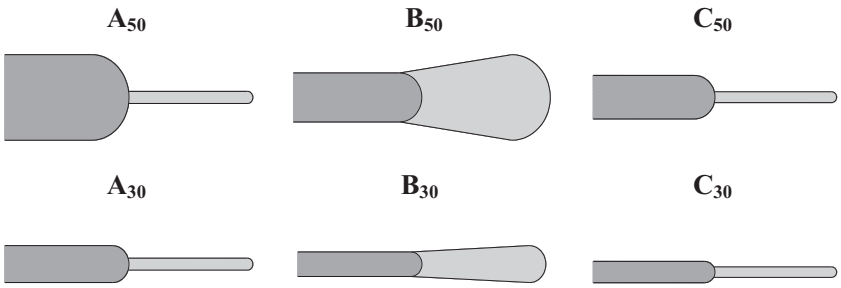

Fig. 16. Crack tip opening displacement (CTOD) for K_{min}.

(i) During the steady-state regime of cracking associated with the Paris law, the fatigue crack growth (FCG), da/dN, is mainly governed by the stress intensity factor (SIF) range ΔK and it is hardly ever affected by any changes in the maximum SIF K_{max}.
(ii) The sudden decrease of either the maximum SIF K_{max} or the SIF range ΔK generates a transient state in the FCG curve da/dN–ΔK. Such a transient situation evolves towards a steady-state regime of cracking linked to the Paris law.
(iii) The overload retardation effect (ORE), caused by the sudden load decrease between the two loading sequences, is more intense when the amount of load decrease is higher or when the initial SIF K_0 during the second stage diminishes.
(iv) There is almost no ORE in the case of B-type tests with sudden decrease of the unique parameter $\Delta\sigma$. Generally speaking, the ORE is higher in C-type tests (sudden decrease of both $\Delta\sigma$ and σ_{max}) than in A-type tests (sudden decrease of only σ_{max}).
(v) The size of the plastic zone can be estimated from the two key driving forces for FCG, K_{max} and ΔK. The sudden decrease of $K_{max}\Delta K$ generates a transition from the primary to the secondary plastic zone, thereby producing the afore-said ORE.
(vi) A basic assumption of this paper is based in the ratio between the primary and the secondary plastic zones, considering that these amounts are one of the key variables governing the transient regime of cracking and thus the ORE.
(vii) The fatigue fracture surface in pearlite exhibits a ductile micro-tearing pattern, whose appearance and micro-roughness change with K_{max}. On the other hand, ΔK hardly affects the appearance of the fatigue crack surface.
(viii) In A- and C-type tests, the sudden load decrease causes a zone whose fractography is that of fatigue initiation and whose appearance resembles *tearing topography surface* or TTS, associated with slow crack growth produced by micro-plastic tearing events.
(ix) In addition to the influence of the sizes of the primary and the secondary plastic zones, the ORE can also be attributed to the sudden decrease of the crack tip opening displacement (CTOD) causing a similar phenomenon to that of crack growth from a notch.

Acknowledgements

The authors wish to acknowledge the financial support provided by the following Spanish Institutions: Ministry for Science and Technology (MICYT; Grant MAT2002-01831), Ministry for Education and Science (MEC; Grant BIA2005-08965), Ministry for Science and Innovation (MICINN; Grants BIA2008-06810 and BIA2011-27870), *Junta de Castilla y León* (JCyL; Grants SA067A05, SA111A07 and SA039A08), and the steel supplied by TREFILERÍAS QUIJANO (Cantabria, Spain).

References

[1] Skorupa M. Load interaction effects during fatigue crack growth under variable amplitude loading – a literature review. Part I: empirical trends. Fatigue Fract Eng Mater Struct 1998;21:987–1006.
[2] Pommier S, Bompard P. Bauschinger effect of alloys and plasticity-induced crack-closure: a finite element analysis. Fatigue Fract Eng Mater Struct 2000;23:129–39.
[3] Ogura K, Ohji K. FEM analysis of crack closure and delay effect in fatigue crack growth under variable amplitude loading. Eng Fract Mech 1977;9:471–80.
[4] Matsuoka S, Tanaka K. The retardation phenomenon of fatigue crack growth in HT80 steel. Eng Fract Mech 1976;8:507–23.
[5] Ward-Close CM, Blom AF, Ritchie RO. Mechanisms associated with transient fatigue crack growth under variable-amplitude loading: an experimental and numerical study. Eng Fract Mech 1989;32:613–38.
[6] Pommier S, de Freitas M. Effect of fatigue crack growth of interactions between overloads. Fatigue Fract Eng Mater Struct 2002;25:709–22.
[7] Makabe C, Purnowidodo A, McEvily AJ. Effects of surface deformation and crack closure on fatigue crack propagation after overloading and underloading. Int J Fatigue 2004;26:1341–8.
[8] Suresh S. Micromechanisms of fatigue crack growth retardation following overloads. Eng Fract Mech 1983;18:577–93.
[9] Suresh S, Ritchie RO. On the influence of fatigue underloads on cyclic crack growth at low stress intensities. Mater Sci Eng 1981;51:61–9.
[10] Vasudevan AK, Sadananda K, Glinka G. Critical parameters for fatigue damage. Int J Fatigue 2001;23:S39–53.
[11] Sadananda K, Vasudevan AK. Crack tip driving forces and crack growth representation under fatigue. Int J Fatigue 2004;26:39–47.
[12] Toribio J, Ovejero E. Microstructure orientation in a pearlitic steel subjected to progressive plastic deformation. J Mater Sci Lett 1998;17:1045–8.
[13] Toribio J, Ovejero E. Microstructure evolution in a pearlitic steel subjected to progressive plastic deformation. Mater Sci Eng A 1997;234–6:579–82.
[14] Toribio J, Ovejero E. Effect of cold drawing on microstructure and corrosion performance of high-strength steel. Mech Time-Depend Mater 1998;1:307–19.
[15] Toribio J, Ovejero E. Effect of cumulative cold drawing on the pearlite interlamellar spacing in eutectoid steel. Scripta Mater 1998;39:323–8.
[16] Toribio J, Matos JC, González B. Micro- and macro-approach to the fatigue crack growth in progressively drawn pearlitic steels at different *R*-ratios. Int J Fatigue 2009;31:2014–21.
[17] Jones R, Farahmand B, Rodopoulos CA. Fatigue crack growth discrepancies with stress ratio. Theor Appl Fract Mech 2009;51:1–10.
[18] Forth SC, James MA, Johnston WM, Newman JC Jr. Anomalous fatigue crack growth phenomena in high-strength steel. In: Proceedings of the 11th international conference on fracture (ICF 11), Turin, Italy 2005.
[19] Toribio J, González B, Matos JC. Fatigue crack propagation in cold drawn steel. Mater Sci Eng A 2007;468–70:267–72.
[20] Yarema SY. Test method for the determination of crack growth rates and crack growth resistance under cyclic loading. National Karpenko Physico-Mechanical Institute; 1994.
[21] Toribio J, González B, Matos JC. Transient and steady state regimes of fatigue crack growth in high strength steel. Key Eng Mater 2013;525–6:553–6.
[22] Irwin GR. Plastic zone near a crack and fracture toughness. Mechanical and metallurgical behaviour of sheet materials. In: Proceedings of the 7th Sagamore Ordnance, materials research conference. Syracuse University, New York, USA 1960. p. 63–71.
[23] Dugdale DS. Yielding of steel sheets containing slits. J Mech Phys Solids 1960;8:100–4.
[24] Thompson AW, Chesnutt JC. Identification of a fracture mode: the tearing topography surface. Metall Trans A 1979;10:1193–6.
[25] Suresh S. Fatigue of materials. 2nd ed. New York: Cambridge University Press; 1998.
[26] Toribio J, Kharin V. Plasticity-induced crack closure: a contribution to the debate. Eur J Mech A Solids 2011;30:105–12.
[27] Toribio J, Kharin V. Simulations of fatigue crack growth by blunting–re-sharpening: plasticity induced crack closure vs. alternative controlling variables. Int J Fatigue 2013;50:72–82.